



Photodegradation of Synozol Red HF-6BN on g-C₃N₄/Halloysite nanocomposites

Hoa Thi Nguyen, Xuan Nui Pham*

Department of Chemical Engineering, Hanoi University of Mining and Geology, 18-Pho Vien, Duc Thang, Bac Tu Liem District, Hanoi, Vietnam.

* Email: phamxuannui@humg.edu.vn

ARTICLE INFO

Received: 11/7/2021

Accepted: 10/8/2021

Published: 20/8/2021

Keywords:

Photocatalyst, g-C₃N₄, Halloysite
 Nanocomposite, Synozol red HF-6BN

ABSTRACT

In the research, graphitic carbon nitride (g-C₃N₄) was synthesized using modified halloysite via a calcination method. The improvement of photocatalytic activity mainly benefits from the reduced e⁻/h⁺ pairs recombination rate, the improved electron separation yield. The photocatalytic activity of nanocomposite was evaluated through the Synozol red HF-6BN dye degradation, the degradation efficiency approached 99% after 30 mins irradiation under the solar light, and the performance is slightly reduced to 94 % after three consecutive tests. These results have demonstrated an effective method to synthesize g-C₃N₄ photocatalysts with nanostructures using crude clay minerals.

Introduction

In recent years, there has been much research using different methods to treat toxic organic compounds in water such as mechanical, biological, physical chemistry methods,... The biological method is evaluated as the most economical when compared to physical chemistry, mechanical methods [1]. However, their applicability is limited due to the long processing time and ineffective with high molecular structure [2]. Recently, photocatalysis was nominated as a superior method that active under visible light, capable of degradation organic compounds, thoroughly degradation complex colored substances. In addition, this method has other advantages as consuming less energy, ease of use and less toxic [3]. Most photocatalytic materials are based on metal oxides, typically TiO₂ [4], Fe₂O₃ [4], CdS [5], Bi₂WO₆ [6] – these substances are active only under UV light, accounting for only 5% of solar energy. Furthermore, metal oxides cannot respond to the sustainability requirement due to their high cost, and scarcity [7]. Hence, the

researchers find a new type of sustainable, inexpensive catalysts and can operate under visible light. Non-metallic semiconductors–graphitic carbon nitride (g-C₃N₄) receives much attention because of their photocatalytic reactivity in the wide light region, low fabrication costs, ease of synthesis, and possible green synthesis, non-toxic, chemical stability, and narrow bandgap energy (approximately 2.7 eV) [7]. g-C₃N₄ is easily prepared by thermal polymerization from nitrogen-rich precursors such as melamine, dicyandiamide, cyanamide, urea, thiourea, and ammonium thiocyanate [8]. However, the disadvantages of g-C₃N₄ have limited their applications in the field of photocatalyst like low surface area [9], the fast recombination rate of the e⁻/h⁺ pairs [10], low electron separation yield [11]. To improve these limitations, several methods have been proposed to create mesoporous materials [12], doped with metallic or non-metallic elements [13][14], magnetized with the magnetic material [15][16].

In addition, the use of natural mineral sources as support agents is also a new approach direction.

<https://doi.org/10.51316/jca.2021.064>

Halloysite ($\text{Al}_2\text{Si}_2\text{O}_5(\text{OH})_4 \cdot n\text{H}_2\text{O}$, HNT) is a natural aluminosilicate clay mineral and usually exists as tubes. Halloysite tubes have different surface chemistry on the internal and external: the internal surface of HNT is composed of gibbsite octahedral sheet (Al-OH) groups and is positively charged, while its negatively charged outer surface is consist of siloxane groups (Si-O-Si). Halloysite tubes are rolled to form cylinders as a result of the strain caused by lattice mismatch between adjacent silicon dioxide and aluminum oxide sheets [17].

The combination of $\text{g-C}_3\text{N}_4$ photocatalyst and halloysite tubes was synthesized by Wenbin Wang et al. [18] through vapor deposition method. The results show that the separation efficiency of H_2 from water is $633 \mu\text{mol g}^{-1} \text{h}^{-1}$ under light irradiation, the higher 14.3 times that pure $\text{g-C}_3\text{N}_4$. The improvement of the photocatalytic activity was mainly due to the enlarged specific surface area and the decrease in the photogenerated electron-hole pairs recombination rate when $\text{g-C}_3\text{N}_4$ was modified by halloysite tubes. This study is the first step for the synthesis of composite materials based on $\text{g-C}_3\text{N}_4$ and halloysite clay minerals for environmental treatment.

Hence, a facile calcination route was proposed to synthesize the novel visible-light-responsive $\text{g-C}_3\text{N}_4/\text{HNT}$ composite. In this study, the combining process of $\text{g-C}_3\text{N}_4$ with halloysite tubes was researched. The photodegradation tests were performed on Synozol red HF-6BN and the proposable mechanisms of enhancement of photocatalytic activity were also investigated.

Experimental

Reagents



Figure 1: Structure of Synozol red HF-6BN

Urea (>99%), halloysite (>99%), H_2O_2 (30%), and Synozol red HF-6BN dye (>99%) were supplied by

Sigma-Aldrich. All chemicals and reagents in this research used without any further purification.

Preparation of graphitic carbon nitride ($\text{g-C}_3\text{N}_4$)

The $\text{g-C}_3\text{N}_4$ was obtained through calcination with urea as a precursor. Typically, 5 g urea was put into a ceramic crucible, placed in a muffle furnace and heated at $500 \text{ }^\circ\text{C}$ for 2 h at the heating of $5 \text{ }^\circ\text{C} \cdot \text{min}^{-1}$ and then cooled to room temperature. The $\text{g-C}_3\text{N}_4$ has obtained a yellow powder.

Preparation of $\text{g-C}_3\text{N}_4/\text{HNT}$ composite

The $\text{g-C}_3\text{N}_4/\text{HNT}$ composite was synthesized by calcination method. Typically, three different amounts of urea (2 g, 3 g, and 4 g with weight percentages of $\text{g-C}_3\text{N}_4$ were 30%, 40%, 50%, respectively) and 2 g HNT was put into a ceramic crucible with a cover, placed in a muffle furnace and heated at $500 \text{ }^\circ\text{C}$ for 2h at the heating of $5 \text{ }^\circ\text{C} \cdot \text{min}^{-1}$ and then cooled to room temperature. The obtained composites were labeled as 30%, 40%, and 50% $\text{g-C}_3\text{N}_4/\text{HNT}$.

Characterization

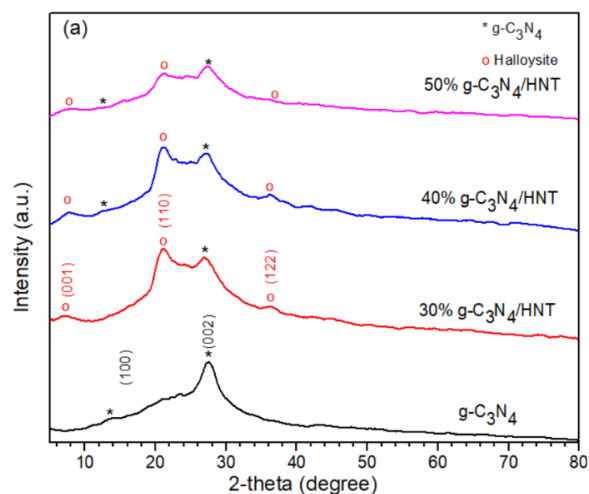
The crystal lattice structure of the synthesized samples was determined by X-ray powder diffraction (XRD) using a D8 ADVANCE system (Cu $\text{K}\alpha_1$ copper radiation, $\lambda = 0.154 \text{ nm}$, 3° min^{-1} scanning speed, Bruker, Germany). Surface morphology was observed by a scanning electron microscope (S-4800, Hitachi). The Fourier transform infrared spectra (FT-IR) were measured with an FT-IR Affinity-1S (SHIMADZU). The UV-vis diffuse reflectance (UV-vis DRS) and were recorded with the UV-2600 spectrophotometer (Shimadzu). The Brunauer-Emmett-Teller (BET) specific surface area was determined at liquid-nitrogen temperature (77 K) using the N_2 adsorption-desorption technique on a ChemBET-3030 system.

Photocatalytic experiments

Photocatalytic activity of the sample was evaluated by degradation of Synozol red HF-6BN under solar irradiation. Typically, 100 mg of the catalyst was dispersed in 30 mL of the dye solution. The solution mixture was placed in the dark for 30 mins to reach the adsorption-desorption equilibrium. The initial concentration (C_0) was taken at this point. Then, the mixture was illuminated under solar light for 30 mins. After every 5 mins, the small quantity of the solution

was taken and measured under UV-Vis spectrometer to record the concentration (C_t) at maximum wavelength $\lambda = 541$ nm. The conversion of dye was calculated using Equation 1:

$$H\% = \frac{(C_o - C_t)}{C_o} \times 100 \quad (1)$$



Where: C_o is the initial dye concentration (ppm)
 C_t is the concentration of dye at time t (ppm)

Result and discussion

Photocatalyst characterization

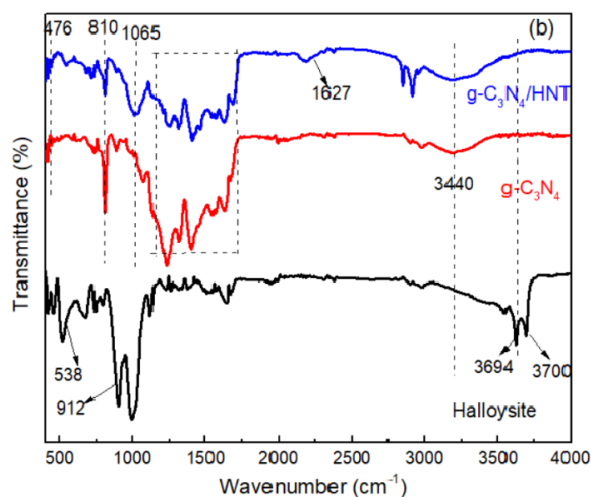


Figure 2: (a) XRD patterns of $g-C_3N_4$, 30-50% $g-C_3N_4$ /HNT composite, and (b) FTIR spectra of halloysite, $g-C_3N_4$, 40% $g-C_3N_4$ /HNT composite

The crystal structure and phase composition of the samples were characterized by XRD. As shown in Figure 2 (a), $g-C_3N_4$ has two distinct diffraction peaks at 13.2° and 27.3° , which are corresponding to the (100) and (002) lattice planes (JCPDS 87-1526) [19]. The weak diffraction peak located at 13.2° belongs to the in-plane repeat of tris-triazine and the stronger diffraction peak located at 27.3° is attributed to the interlayer stacking of aromatic segments, respectively, indicating the fabricated $g-C_3N_4$ has the characteristics of graphite [20]. The XRD patterns of 30-50% $g-C_3N_4$ /HNT composites are similar to that of $g-C_3N_4$, and the characteristic peaks of halloysite were observed at $2\theta = 8.84^\circ, 22.96^\circ, 35.48^\circ$, which corresponded to the (001), (110), (122) [21]. The reduction in the intensity of the (100) peak in $g-C_3N_4$ indicates the decreased planar size of the layer [22]. Consequently, 40% $g-C_3N_4$ /HNT composite was used to evaluate the properties of the composite. The Fourier transformed infrared (FTIR) spectra (Figure 2 (b)) show that the peaks located at $1200-1700\text{ cm}^{-1}$ (C=N and C-

N stretching vibration modes) [23]. The absorption bands at $3000-3500\text{ cm}^{-1}$ were assigned to the O-H of absorbed water and N-H of surface uncondensed amine groups. The peaks that appeared at 810 and 891 cm^{-1} could be attributed to the stretching vibration bands of the C-N to the characteristic breathing vibration of the triazine unit. This indicates that modification of $g-C_3N_4$ by halloysite do not change the main feature of $g-C_3N_4$.

The morphologies of halloysite support and 40% $g-C_3N_4$ /HNT were observed by SEM and TEM images (shown in Figure 3). Figure 3 (a,b,e) show the pure HNT, it is clear that HNTs display a cylindrical-shaped tubular structure which aligned randomly, with the length of nanotubes are around $0.2-1.2\text{ }\mu\text{m}$. It can be clearly observed that the surface of nanotubes is level and smooth. With 40% $g-C_3N_4$ /HNT composite, the halloysite retained its nanotube morphology after the dispersal process while its outer surface became rough due to the deposition of $g-C_3N_4$, as observed by SEM and TEM images (Figure 3 c,d,f).

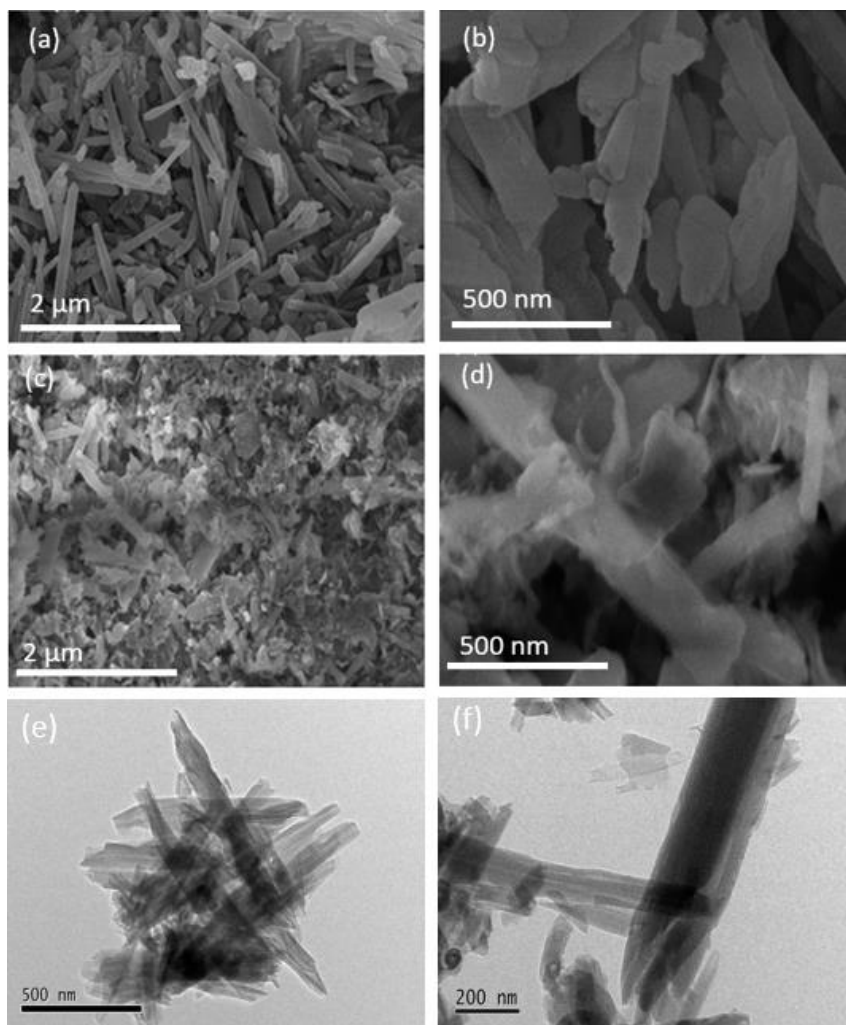


Figure 3: SEM images of (a,b) HNT, (c,d) 40% g-C₃N₄/HNT composite. TEM images of (e) HNT and (f) 40% g-C₃N₄/HNT composite

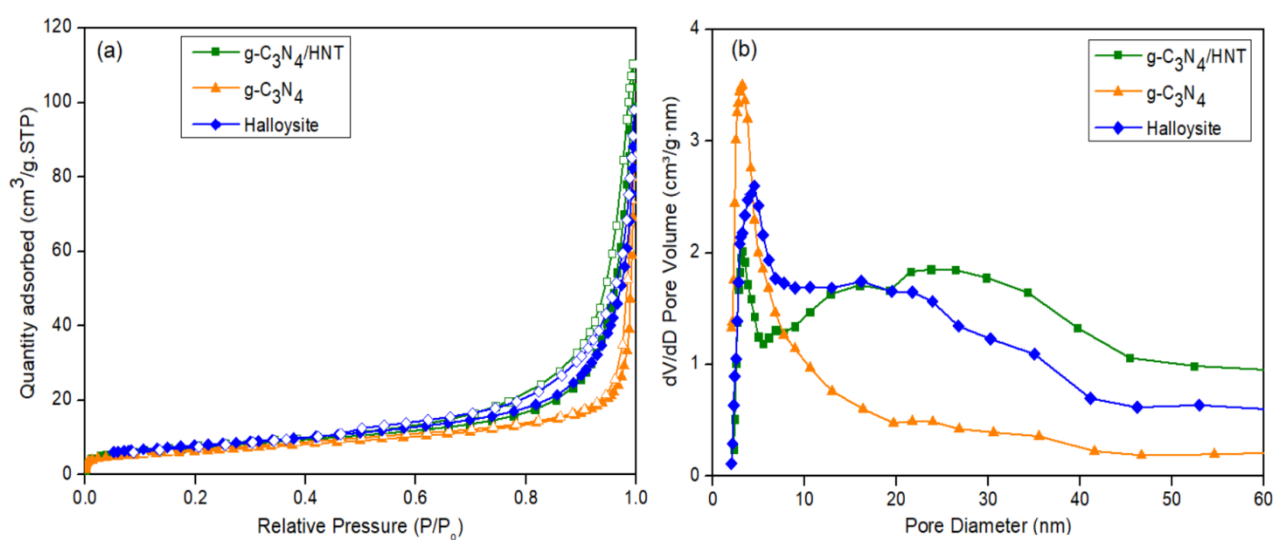


Figure 4: (a) N₂ adsorption-desorption isotherms at 77K and (b) the pore size distribution curves of halloysite, g-C₃N₄ and 40% g-C₃N₄/HNT composite

Figure 4 displays the N₂ adsorption-desorption isotherms of the halloysite, g-C₃N₄ and 40% g-C₃N₄/HNT samples and the corresponding pore size distributions. As shown in Figure 4. (a), these three adsorption-desorption isotherms exhibit typical type IV profiles with distinct hysteresis loops of Type H4 according to the International Union of Pure and Applied Chemistry (IUPAC) classification, indicating mesoporous structures of these two photocatalysts. In addition, the pore size distributions of the halloysite, g-C₃N₄ and 40% g-C₃N₄/HNT samples display a wide range of pore diameter from 2-40 nm, suggesting the

existence of mesopores. As shown in Table 1, the obtained BET specific surface area, average pore diameter, and pore volume of halloysite are 28.02 m².g⁻¹, 25 nm, and 0.14 cm³.g⁻¹, which is higher than pure g-C₃N₄ (20.36 m².g⁻¹, 15 nm, 0.106 cm³.g⁻¹), whereas those of 40% g-C₃N₄/HNT are 25.84 m².g⁻¹, 22 nm, and 0.17 cm³.g⁻¹, respectively. It can be seen that the significant decrease in surface area and pore size of g-C₃N₄/HNT might be attributed to the filling of both micropores and mesopores of the halloysite by g-C₃N₄.

Table 1: Pore structure parameters of the halloysite and 40% g-C₃N₄/HNT composite

Sample	S _{BET} (m ² .g ⁻¹)	D _{pore} (nm)	V _{pore} (cm ³ .g ⁻¹)
Halloysite	28.02	25	0.14
g-C ₃ N ₄	20.36	15	0.106
40% g-C ₃ N ₄ /HNT	25.84	22	0.17

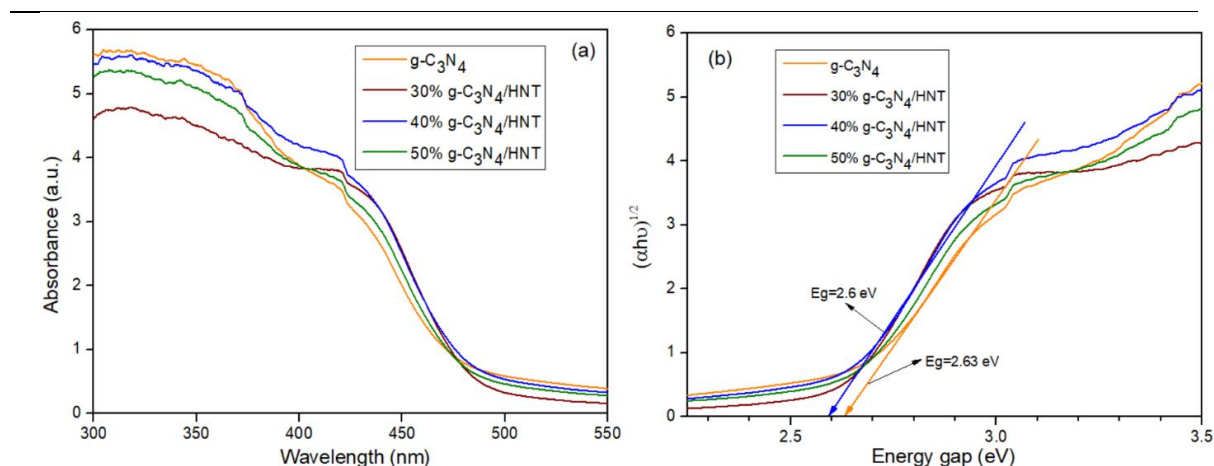


Figure 5: UV-vis adsorption spectra (a) and Tauc plots of the UV-Vis spectra (B) of the as-prepared photocatalysts

In order to investigate the optical properties and band structure of as-prepared composite photocatalysts, the g-C₃N₄, and 30-50% g-C₃N₄/HNT were carried out by UV-vis diffuse reflectance spectra (DRS) in Figure 5. For the pure g-C₃N₄, a band edge is observed at 485 nm, which is consistent with previous reports [24]. Here, the estimated adsorption edge for 40% g-C₃N₄/HNT is 495 nm, which is significantly higher than those for 30% g-C₃N₄/HNT (492 nm) and 50% g-C₃N₄/HNT (489 nm).

The increased optical adsorption of g-C₃N₄/HNT should be attributed to the presence of halloysite nanotubes, which enhanced visible light adsorption ability, leading to the receiving of greater light irradiation in unit time. In addition, the band gap (E_g)

of the as-prepared composite photocatalysts can be calculated from the following Kubelka-Munk equation:

$$\alpha h\nu = A(h\nu - E_g)^{n/2} \quad (2)$$

Where E_g is the band-gap energy of the semiconductor, A is the adsorption constant, h is Planck's constant, and α and ν represent the adsorption coefficient and the frequency, respectively, n is 1 for the direct transition. Therefore, the bandgap energies of the pure g-C₃N₄, 30-50% g-C₃N₄/HNT samples were obtained from a plot of (αhν)^{1/2} versus hν (Figure 5 (b)) as 2.63, 2.61, 2.60, 2.62 eV, respectively. The presence of HNT as a support, which contributed to the red-shift of the absorption onset, result in the narrow band gap of the g-C₃N₄/HNT composite.

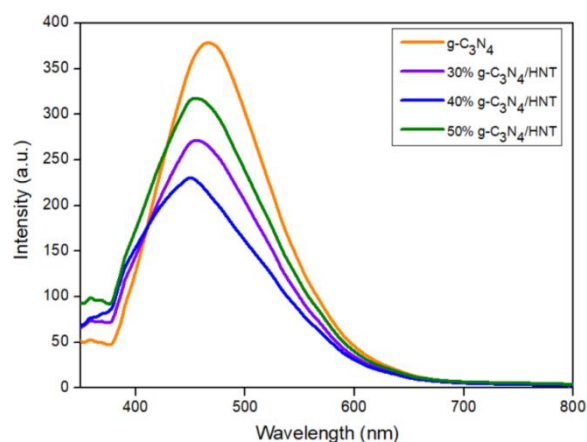


Figure 6: Photoluminescence spectra of $g\text{-C}_3\text{N}_4$, and 30-50% $g\text{-C}_3\text{N}_4/\text{HNT}$ photocatalysts

Photoluminescence spectroscopy (PL) was implemented to investigate the carrier separation efficiency of photocatalytic composites. The higher intensity in the emission peak the more rapid recombination of the photoexcited electron-hole pairs [25]. As can be seen in Figure 6, the PL emission peaks at between 400 and 500 nm are observed in all the samples with the highest intensity observed in $g\text{-C}_3\text{N}_4$, followed by 30-50% $g\text{-C}_3\text{N}_4/\text{HNT}$, which is in good agreement with the analysis of UV-Vis DRS. The results indicate the enhanced separation rates of electron-

hole pairs and the reduced charge transport distance in the composite.

Photocatalytic activity test

According to the previous study [26], halloysite can't be excited by visible light irradiation, but halloysite shows excellent adsorption ability with anion dyes. Because the inner surface of the halloysite tube is composed of Al-OH, which create electro-static attraction between O-H groups and SO_3^- group of the Synozol red HF-6BN.

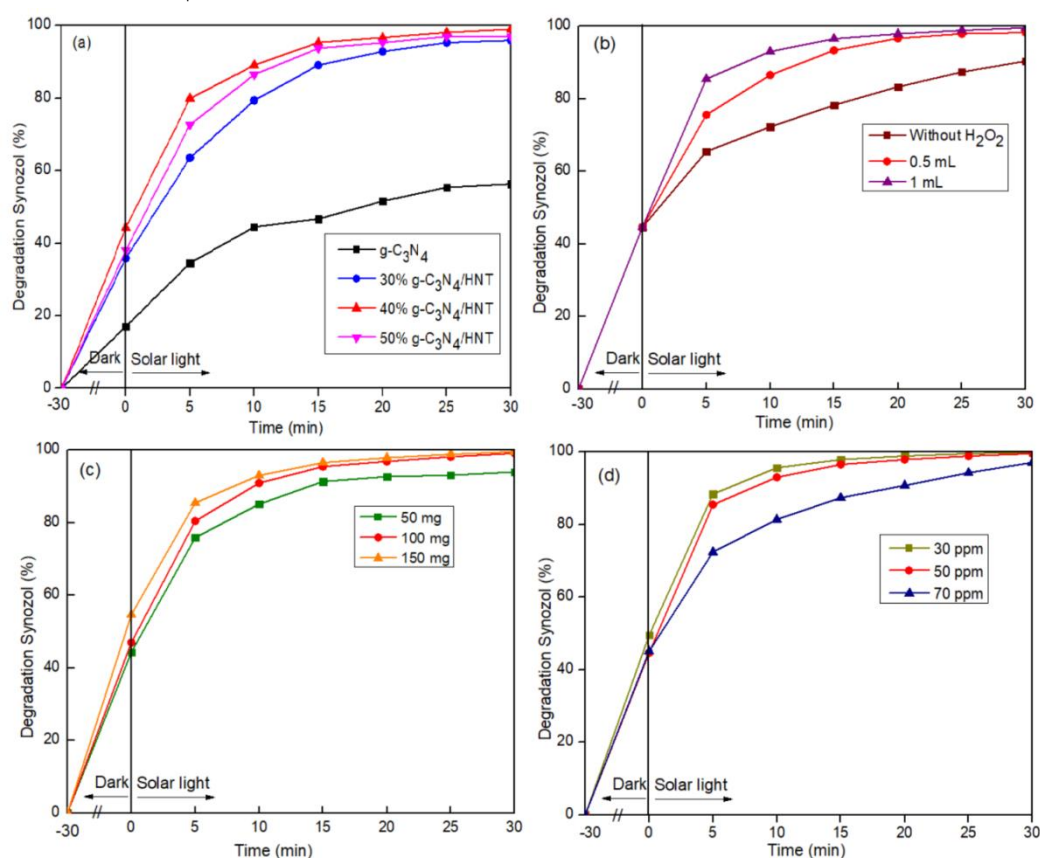


Figure 7: Photodegradation of Synozol red HF-6BN under various reaction conditions of (a) mass contents of $g\text{-C}_3\text{N}_4$, (b) concentration H_2O_2 , (c) photocatalytic dosages, (d) concentration of Synozol red HF-6BN

Effect of g-C₃N₄ contents

Figure 7 (a) illustrates the photodegradation rate of g-C₃N₄/HNT with different content of g-C₃N₄ via degrading Synozol red HF-6BN. From Figure 7 (a), the degradation of HF-6BN with various g-C₃N₄ content can be seen clearly that about 56% HF-6BN was degraded with g-C₃N₄ material after 30 mins under solar light irradiation, which might be due to the fast recombination of photogenerated electrons and holes and low surface area limiting the photocatalytic ability of the g-C₃N₄. In addition, the highest photocatalytic activity of 40% g-C₃N₄/HNT reached at 99% in 30 mins under solar light irradiation which is evidently higher than 30% g-C₃N₄/HNT (95%) and 50% g-C₃N₄/HNT (about 97%). These results are attributed to the excess mass of g-C₃N₄ agglomerates, preventing the formation of photogenerated electron-holes. Moreover, these indicating that the g-C₃N₄ composited with HNT can actually enhance the visible light response ability and photocatalytic activity.

Effect of H₂O₂ concentration

The photocatalytic activity of the 40% g-C₃N₄/HNT catalyst was investigated during the photodegradation of Synozol red HF-6BN in the absence or presence of H₂O₂. As shown in Figure 7 (b), after 30 mins of irradiation with solar light, about 98% of HF-6BN was degraded in the presence of the 0.5 mL H₂O₂ and about 99% of HF-6BN was degraded by the presence

of the 1 mL H₂O₂, while approximately 90% of HF-6BN was decomposed in the absence of H₂O₂. This result also implied that the assistance of H₂O₂ was needed for the degradation of HF-6BN over the g-C₃N₄/HNT.

Effect of photocatalyst dosages

The influence of the different dosages of 40% g-C₃N₄/HNT composite was also investigated under the same reaction conditions. Figure 7 (c) shows that the highest photocatalytic efficiency reached 99% after 30 mins corresponding to 100 mg of the catalyst. However, if the amount of catalyst continually increased, the interaction among the outer layers of the material reduced the photon formation of the inner layers, which led to a decrease in the number of e⁻/h⁺ pairs as well as the photocatalytic efficiency [27].

Effect of Synozol red HF-6BN dye concentration

The initial concentration of Synozol red HF-6BN was used to investigate photocatalytic activity of 40% g-C₃N₄/HNT as shown in Figure 7 (d). When the initial concentration of HF-6BN increased from 30 ppm to 70 ppm, the photocatalytic efficiency slightly decreased from 99% to 97%, implying that a high initial dye concentration could decrease the transmission opportunity and the part of the photon, thereby reducing the penetration rate of the solar light irradiation in the contaminant solution [28].

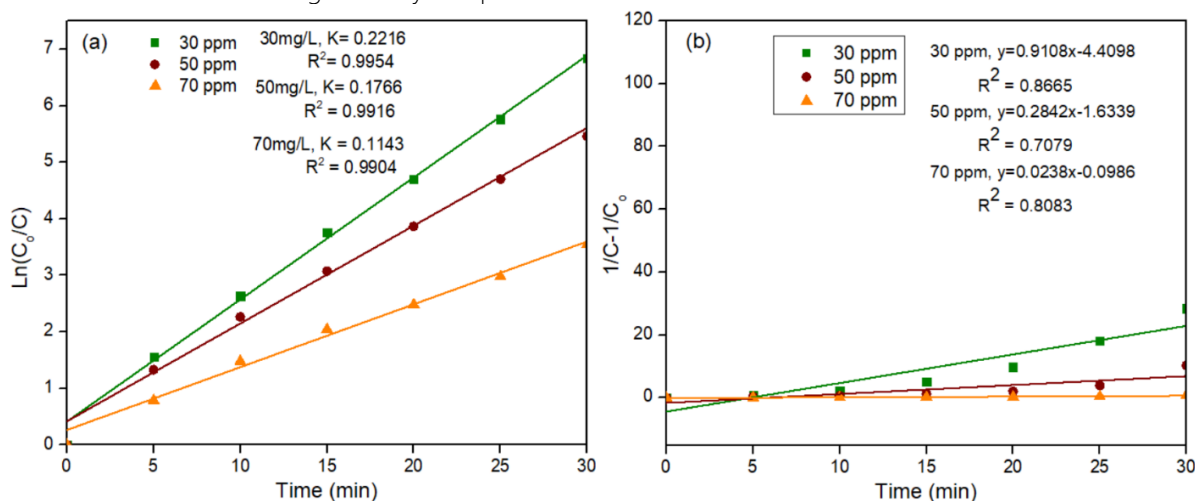


Figure 8: Plot of (a) the pseudo-first order and (b) pseudo-second order kinetic model for the photodegradation Synozol red HF-6BN over 40% g-C₃N₄/HNT composite

The kinetics of the Synozol red HF-6BN photodegradation were modeled based on an operating temperature of 30°C, 100 mg of the as-

synthesized 40% g-C₃N₄/HNT composite, and a pH of 6.5, as shown in Eq.(3,4).

$$-\ln\left(\frac{C_t}{C_o}\right) = k_p t \quad (3) \text{ and } \frac{1}{C_t} - \frac{1}{C_o} = kt \quad (4)$$

Where C_t and C_o are the concentration at time t and initial time, respectively, k_p is the first-order reaction rate constant, k is the pseudo-second-order reaction rate constant, and t is the irradiation time. We observed in Figure 8 that the regression coefficient values for each concentration in the case of the

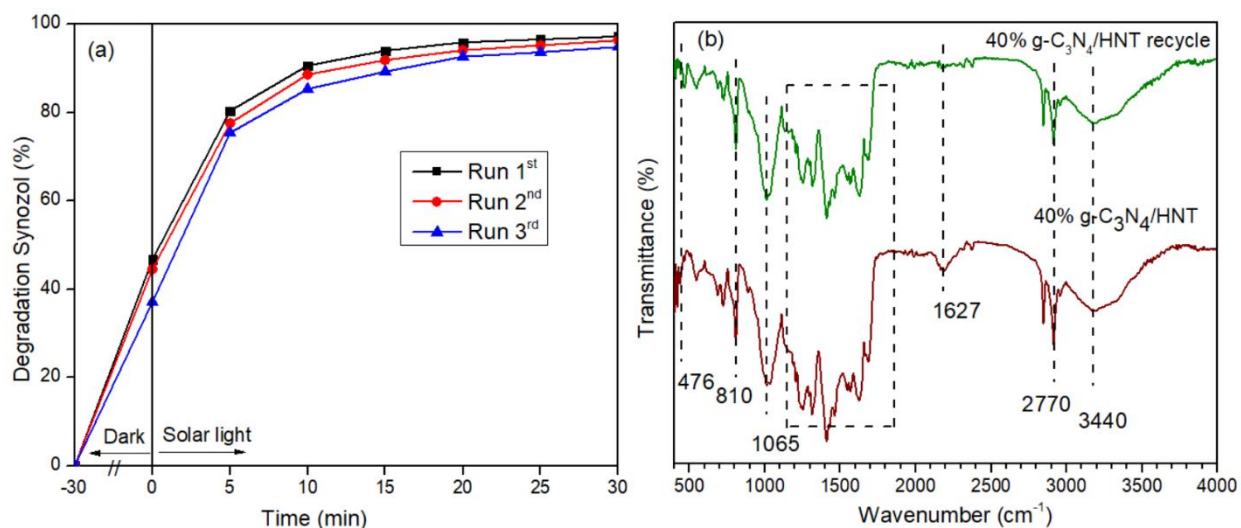


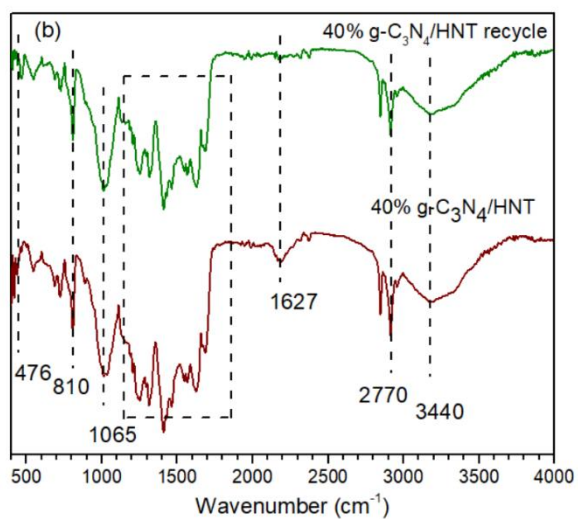
Figure 9: (a) Cycling runs of the photodegradation of Synozol red HF-6BN over 40% g-C₃N₄/HNT, and (b) FT-IR spectra of fresh and used 40% g-C₃N₄/HNT

Stability is very important evidence to judge the quality of the photocatalyst and for further environmental application. The stabilities of the 40% g-C₃N₄/HNT composite photocatalyst were investigated by multicycle repeated experiments for Synozol red HF-6BN degradation under solar light irradiation. The test results are shown in Figure 9 (a), indicating that the photocatalytic activity of this catalyst only slightly decreased (95% remaining) after three consecutive tests under the experimental conditions at which the optimal degradation rate was obtained. Figure 9 (b) presented the results of the FT-IR spectra analysis before and after three consecutive tests and the key g-C₃N₄ and HNT peaks are observed via comparing with the initial figure. The intensity of the used 40% g-C₃N₄/HNT only slightly lower than that before degradation. All the above results demonstrate the excellent stability of the catalyst during photodegradation.

As discussed above, three main reasons for the increase in the photocatalytic efficiency of coupled g-C₃N₄/HNT composites are: (i) the absorption edges of g-C₃N₄/HNT composites shifts significantly to longer

wavelengths compared with the pure g-C₃N₄, which indicates the composites can be excited by more visible light photons; (ii) the enlarged BET surface of g-C₃N₄/HNT composites, the increased surface area offers more surface active sites for adsorption and photocatalytic reaction; (iii) The electrostatic interaction, the negatively charged halloysite can promote the immigration of electrons and holes, thus suppresses the charge recombination. The mechanism for the enhanced photocatalytic activity is illustrated in Figure 10.

Considering the fact that halloysite is known as a very good electrical insulator, halloysite can't be excited and only g-C₃N₄ can be activated, the electron-holes of g-C₃N₄ have no opportunity to migrate to halloysite and still present on the g-C₃N₄ surface. However, the excited electrons and holes of g-C₃N₄ were driven to separate efficiently because the negatively charged halloysite surface restricted electrons transfer but favored holes migration. Thus, the charge recombination could be easily suppressed, leaving more charge carriers and enhancing the photocatalytic activity.



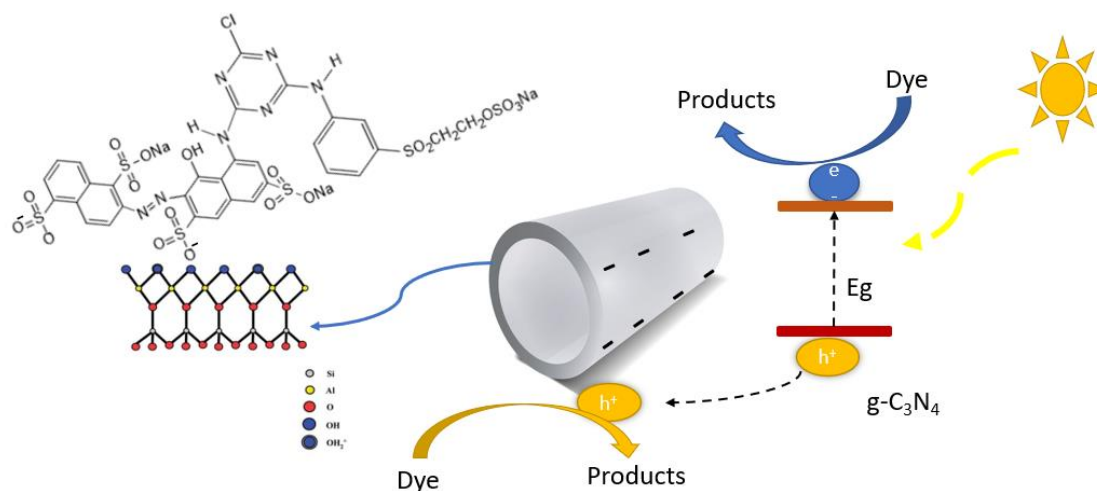


Figure 10: Proposed mechanism for the enhanced charge carriers separation in the $g\text{-C}_3\text{N}_4/\text{HNT}$ composite.

Conclusions

A novel $g\text{-C}_3\text{N}_4/\text{HNT}$ composite was successfully synthesized *via* a calcination method. $g\text{-C}_3\text{N}_4/\text{HNT}$ composites exhibited higher photocatalytic activity in the degradation of Synozol red HF-6BN. Specifically, the highest Synozol red HF-6BN degradation efficiency using 40% $g\text{-C}_3\text{N}_4/\text{HNT}$ composite reached 99% after 30 mins under solar light irradiation. The significant enhancement in the photocatalytic performance of $g\text{-C}_3\text{N}_4/\text{HNT}$ composites is ascribed not only to its adsorptive and enhanced absorptivity under visible light but also to the electrostatic interaction between $g\text{-C}_3\text{N}_4$ and negatively charged halloysite surface, this can promote the efficient migration of photogenerated electrons and holes of $g\text{-C}_3\text{N}_4$ and consequently improves the photocatalytic activity.

Acknowledgments

Hoa Thi Nguyen was funded by Vingroup Joint Stock Company by the Domestic Master/PhD Scholarship Programme of Vingroup Innovation Foundation (VINIF), Vingroup Big Data Institute (VINBIGDATA), code VINIF. 2020. ThS. 19

References

1. C. Fernández, M. S. Larrechi, and M. P. Callao, An analytical overview of processes for removing organic dyes from wastewater effluents, *TrAC - Trends in Analytical Chemistry* (2010). <https://doi.org/10.1016/j.trac.2010.07.011>
2. T. L. H. Vũ Thị Bích Ngọc, Hoàng Thị Hương Huế, "Xử lý màu nước thải dệt nhuộm thực tế bằng phương pháp oxy hóa nâng cao," *Tạp chí Khoa học*
3. Nguyễn Kim Suyển, Nghiên cứu điều chế, khảo sát cấu trúc và tính chất của titan dioxit kích thước nano met được biến tính bằng nito, Luận văn thạc sĩ, Đại học Khoa học tự nhiên - Đại học Quốc gia Hà Nội (2010).
4. K. Nakata and A. Fujishima, TiO_2 photocatalysis: Design and applications, *J. Photochem. Photobiol. C Photochem. Rev.*, vol. 13, no. 3 (2012) 169–189.
5. L. Cheng, Q. Xiang, Y. Liao, and H. Zhang, CdS-based photocatalysts, *Energy Environ. Sci.*, vol. 11, no. 6 (2018) 1362–1391.
6. C. Huang, L. Chen, H. Li, Y. Mu, and Z. Yang, Synthesis and application of Bi_2WO_6 for the photocatalytic degradation of two typical fluoroquinolones under visible light irradiation, *RSC Adv.*, vol. 9, no. 48 (2019) 27768–27779.
7. J. Zhang and H. Sun, Carbon nitride photocatalysts, in *Multifunctional Photocatalytic Materials for Energy*, Elsevier (2018) 103–126.
8. Y. Wang, X. Wang, and M. Antonietti, Polymeric graphitic carbon nitride as a heterogeneous organocatalyst: From photochemistry to multipurpose catalysis to sustainable chemistry, *Angewandte Chemie - International Edition* (2012) <https://doi.org/10.1002/anie.201101182>
9. I. Papailias, N. Todorova, T. Giannakopoulou, J. Yu, D. Dimotikali, and C. Trapalis, Photocatalytic activity of modified $g\text{-C}_3\text{N}_4/\text{TiO}_2$ nanocomposites for NOx removal, *Catal. Today*, vol. 280 (2017) 37–44.
10. Z. Zhao, Y. Sun, and F. Dong, Graphitic carbon nitride based nanocomposites: A review, *Nanoscale* (2015). <https://doi.org/10.1039/c4nr03008g>
11. J. Liu, S. Xie, Z. Geng, K. Huang, L. Fan, W. Zhou, L. Qiu, D. Gao, L. Ji, L. Duan, L. Lu, W. Li, S. Bai, Z. Liu, W. Chen, S. Feng, and Y. Zhang, Carbon Nitride Supramolecular Hybrid Material Enabled High-

12. Efficiency Photocatalytic Water Treatments, *Nano Lett.*, (2016).
[https:// 10.1021/acs.nanolett.6b03229](https://10.1021/acs.nanolett.6b03229)
13. Q. Han, B. Wang, J. Gao, Z. Cheng, Y. Zhao, Z. Zhang, and L. Qu, Atomically Thin Mesoporous Nanomesh of Graphitic C₃N₄ for High-Efficiency Photocatalytic Hydrogen Evolution, *ACS Nano*, (2016).
[https:// 10.1021/acsnano.5b078](https://10.1021/acsnano.5b078)
14. S. Ma, S. Zhan, Y. Jia, Q. Shi, and Q. Zhou, Enhanced disinfection application of Ag-modified g-C₃N₄ composite under visible light *Appl. Catal. B Environ.*, (2016).
[https:// 10.1016/j.apcatb.2015.12.051](https://10.1016/j.apcatb.2015.12.051)
15. R. Chen, J. Zhang, Y. Wang, X. Chen, J. A. Zapien, and C. S. Lee, Graphitic carbon nitride nanosheet@metal-organic framework core-shell nanoparticles for photo-chemo combination therapy, *Nanoscale*, (2015).
[https:// 10.1039/c5nr04436g](https://10.1039/c5nr04436g)
16. Z. Zhu, Z. Lu, D. Wang, X. Tang, Y. Yan, W. Shi, Y. Wang, N. Gao, X. Yao, H. Dong, Construction of high-dispersed Ag/Fe₃O₄/g-C₃N₄ photocatalyst by selective photo-deposition and improved photocatalytic activity, *Appl. Catal. B Environ.* (2016).
[https:// 10.1016/j.apcatb.2015.09.029](https://10.1016/j.apcatb.2015.09.029)
17. S. Verma, R. B. Nasir Baig, C. Han, M. N. Nadagouda, and R. S. Varma, Magnetic graphitic carbon nitride: Its application in the C-H activation of amines, *Chem. Commun.*, (2015).
[https:// 10.1039/c5cc05895c](https://10.1039/c5cc05895c)
18. E. Abdullayev and Y. Lvov, Halloysite clay nanotubes for controlled release of protective agents, *Journal of Nanoscience and Nanotechnology*. (2011).
[https:// 10.1166/jnn.2011.5724](https://10.1166/jnn.2011.5724)
19. W. Wang, Z. Shu, J. Zhou, T. Li, P. Duan, Z. Zhao, Y. Tan, C. Xie, S. Cui, Halloysite-derived mesoporous g-C₃N₄ nanotubes for improved visible-light photocatalytic hydrogen evolution, *Appl. Clay Sci.*, vol. 158, no. December 2017 (2018) 143–149.
[https:// 10.1016/j.clay.2018.03.018](https://10.1016/j.clay.2018.03.018)
20. S. Cao, J. Low, J. Yu, and M. Jaroniec, Polymeric Photocatalysts Based on Graphitic Carbon Nitride, *Adv. Mater.*, (2015).
[https:// 10.1002/adma.201500033](https://10.1002/adma.201500033)
21. W. Yan, L. Yan, and C. Jing, Impact of doped metals on urea-derived g-C₃N₄ for photocatalytic degradation of antibiotics: structure, photoactivity and degradation mechanisms, *Appl. Catal. B Environ.*, vol. 244 (2019) 475–485.
22. J. M. Falcón, T. Sawczen, and I. V. Aoki, Dodecylamine-loaded halloysite nanocontainers for active anticorrosion coatings, *Front. Mater.*, vol. 2, (2015) 69.
23. P. Qiu, C. Xu, H. Chen, F. Jiang, X. Wang, R. Lu, X. Zhang, One step synthesis of oxygen doped porous graphitic carbon nitride with remarkable improvement of photo-oxidation activity: Role of oxygen on visible light photocatalytic activity, *Appl. Catal. B Environ.*, vol. 206 (2017) 319–327.
24. H. Huang, K. Xiao, N. Tian, F. Dong, T. Zhang, X. Du, Y. Zhang, "Template-free precursor-surface-etching route to porous, thin gC₃N₄ nanosheets for enhancing photocatalytic reduction and oxidation activity," *J. Mater. Chem. A*, vol. 5, no. 33 (2017) 17452–17463.
25. A. Akhundi and A. Habibi-Yangjeh, "Novel magnetically separable g-C₃N₄/AgBr/Fe₃O₄ nanocomposites as visible-light-driven photocatalysts with highly enhanced activities," *Ceram. Int.*, (2015).
[https:// 10.1016/j.ceramint.2014.12.145](https://10.1016/j.ceramint.2014.12.145)
26. H. Shi, G. Chen, C. Zhang, and Z. Zou, Polymeric g-C₃N₄ coupled with NaNbO₃ nanowires toward enhanced photocatalytic reduction of CO₂ into renewable fuel, *ACS Catal.*, (2014).
[https:// 10.1021/cs500848f](https://10.1021/cs500848f)
27. G. Mishra and M. Mukhopadhyay, TiO₂ decorated functionalized halloysite nanotubes (TiO₂@ HNTs) and photocatalytic PVC membranes synthesis, characterization and its application in water treatment," *Sci. Rep.*, vol. 9, no. 1 (2019) 1–17.
28. S. Ahmed, M. G. Rasul, W. N. Martens, R. Brown, and M. A. Hashib, Heterogeneous photocatalytic degradation of phenols in wastewater: A review on current status and developments, *Desalination*. (2010).
[https:// 10.1016/j.desal.2010.04.062](https://10.1016/j.desal.2010.04.062)
29. F. Chen, Q. Yang, Y. Zhong, H. An, J. Zhao, T. Xie, Q. Xu, X. Li, D. Wang, G. Zeng, "Photo-reduction of bromate in drinking water by metallic Ag and reduced graphene oxide (RGO) jointly modified BiVO₄ under visible light irradiation," *Water Res.*, vol. 101, 555–563, 2016.